International Journal of Solids and Structures 48 (2011) 698–705

Contents lists available at ScienceDirect

International Journal of Solids and Structures

journal homepage: www.elsevier.com/locate/ijsolstr

# Impact behavior of honeycombs under combined shear-compression. Part II: Analysis

B. Hou [a,b], S. Pattofatto [b], Y.L. Li [a], H. Zhao [b,*]

[a] School of Aeronautics, Northwestern Polytechnical University, 710072 Xi'an, China

[b] Laboratoire de Mecanique et Technologie, ENS Cachan/CNRS UMR8535/UPMC Parisuniversitas/PRES UniverSud, 61 Avenue du président Wilson, 94235 Cachan Cedex, France

ARTICLE INFO

*Article history:*
Received 25 March 2010
Received in revised form 3 October 2010
Available online 5 November 2010

*Keywords:*
Honeycombs
Combined shear-compression
FEM
Dynamic strength enhancement

ABSTRACT

In this paper, a numerical virtual model of honeycomb specimen as a small structure is used to simulate its combined shear-compression behavior under impact loading. With ABAQUS/Explicit code, the response of such a structure made of shell elements is calculated under prescribed velocities as those measured in the combined shear-compression tests presented in Part I of this study.

The simulated results agree well with the experimental ones in terms of overall pressure/crush curves and deformation modes. It allows for the determination of the separated normal behavior and shear behavior of honeycomb specimen under dynamic combined shear-compression. It is found that the normal strength of honeycombs decreases with increasing shearing load. Quasi-static calculations were also performed and a significant dynamic strength enhancement found in experiments was validated again in the numerical work. A crushing envelope in normal strength vs. shear strength plane was obtained on the basis of these simulations.



## 1. Introduction

Dynamic multiaxial behavior of honeycombs as a basic energy-absorption design parameter is eagerly desired in order to perform numerical simulations for various industrial applications. Many previous works in this domain have been reported in the open literatures and a large number of these works concern mainly the in-plane behavior, and mostly under quasi-static loadings (Gibson and Ashby, 1997; Gibson et al., 1989; Klintworth and Stronge, 1988; Yang and Huang, 2005; Papka and Kyriakides, 1999). However, the most interesting behavior of honeycombs for an energy absorption application is the out-of-plane crushing behavior, especially the one under combined out-of-plane shear-compression which is the most realistic loading mode for such use.

Under quasi-static loadings, some testing methods for the combined shear-compressive loading have been reported (Doyoyo and Mohr, 2003; Mohr and Doyoyo, 2004a; Hong et al., 2006) and they were used to determine the yield envelope of aluminum honeycombs under this particular loading state (Hong et al., 2006; Mohr and Doyoyo, 2004b,c). For examples, (Hong et al., 2006) derived a quadratic yield criterion suitable for orthotropic materials by modifying Hill's quadratic yield criterion. (Mohr and Doyoyo, 2004b,c) suggested a linear fit for the crushing envelope based on their quasi-static calculating results.

Under dynamic loading, many reported works revealed that the strength of honeycombs under uniaxial dynamic compression is higher than under quasi-static loading (Wu and Jiang, 1997; Baker et al., 1998; Harrigan et al., 1999; Goldsmith and Louie, 1995; Goldsmith and Sackman, 1992; Zhao and Gary, 1998; Zhao et al., 2005), even the shock wave effect is not involved (Elnasri et al., 2007). However, the behavior of honeycombs under dynamic multiaxial loading is rarely reported up to now. The main reason for such situations lies in the difficulties to achieve dynamic multiaxial experiments with accurate data measurements.

Some previous work proposed the dynamic multiaxial testing methods using drop-weight or high speed machine (Hong et al., 2008; Chung and Waas, 2002), but the accuracy is not optimal at higher loading rates. In order to improve the measurement accuracy, we proposed in Part I of this study a new testing method using large diameter Hopkinson bar with beveled ends to perform combined shear-compression test under impact loading. It permits to obtain interesting overall pressure/crush curves but can not give a separate normal and pure shear behavior. Thus, with the tests developed in Part I, there is no means to identify directly a given yield criterion.

In Part II of the work, a numerical approach is presented to study a yield criterion. The dynamic and quasi-static combined shear-compression experiments are numerically reproduced with a detailed FEM model for honeycomb specimen. The accuracy of these simulations is validated by comparing the numerical results with the testing ones. Such virtual tests provide a separated normal and shear behaviors of honeycomb specimen, which allow

* Corresponding author. Tel.: +33 1 47 40 20 39; fax: +33 1 47 40 22 40.
*E-mail address:* zhao@lmt.ens-cachan.fr (H. Zhao).

0020-7683/$ - see front matter © 2010 Elsevier Ltd. All rights reserved.
doi:10.1016/j.ijsolstr.2010.11.004

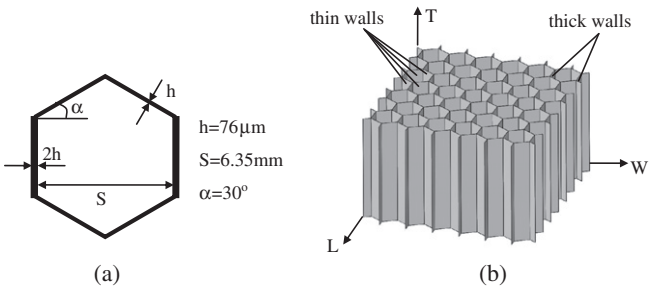


**Fig. 1.** The geometry of unit cell (a) and the constructed honeycomb specimen (b).

for the determination of the yield envelope depicted in terms of the macroscopic shear strength vs. compressive strength.

## 2. Numerical tests of honeycombs under combined shear-compression

Since the study is focused on the behavior of honeycombs under a combined out-of-plane shear-compression, the modeling of the whole testing environment is not necessary. Thus, only detailed honeycomb structures were modeled here and the loading environment was modeled by two rigid planes moving at the velocities measured during real tests. Commercial FEM code of ABAQUS/Explicit was employed for this simulated work.

### 2.1. Numerical specimen

The honeycomb structure studied here has the same geometry as the hexagonal honeycomb used in the experiments in Part I. It is composed of single-thickness walls (or thin walls) and double-thickness walls (or thick walls), and the main geometric parameters were as follows: single wall thickness $h = 76$ μm, expansion angle $\alpha = 30°$, and the minimum cell diameter $S = 6.35$ mm (as shown in Fig. 1(a)).

A complete-model possesses the same size as the specimen employed in experiments, which includes 39 cells on the honeycomb cross-section. The dimensions of the specimen are $25 \times 40 \times 40$ mm in the directions of $T$, $L$ and $W$ respectively (Fig. 1(b)).

The thick walls in a real honeycomb are typically made of two single-thickness thin walls which are bonded together. In this model, we ignore the rare delamination of the bonded interfaces and consider the strength of the adhesive bond as infinite. Thus, the simulations are carried out for a monolithic honeycomb, where the thick walls are represented by a single shell element layer but with a doubled thickness value.

The model is meshed with 4-node doubly curved thick shell elements with a reduced integration, finite membrane strains, active stiffness hour-glass control (S4R) and 5 integration points through the cell wall thickness. In order to determine the appropriate element size, a convergence study was performed among element sizes of 1 mm, 0.5 mm, 0.25 mm and 0.125 mm. It seems that the results converge when the element size is equal to or below 0.25 mm. With the chosen element size of 0.25 mm, our complete-model has totally 232,600 elements.

The numerical specimen is placed between two rigid planes moving with prescribed velocities. The combined shear-compressive loading is realized by applying the real input and output velocities (denoted as $V_{input}$ and $V_{output}$ in Fig. 2) measured in the combined shear-compression experiments reported in Part I of this study. In this model, general contact with frictionless tangential behavior is defined for the whole model excluding the contact pairs of rigid planes and tested honeycomb specimen, which are redefined by surface-to-surface rough contact to make sure that no slippage occurs.

As the real honeycomb is always far from perfect, it includes all kinds of imperfections which affect the initial peak value, but have little influence on the crush behavior at a large strain. These imperfections are due to various reasons, like irregular cell geometry, uneven or pre-buckled cell walls, wall thickness variation etc. Here in this work, we generated the imperfections by preloading the perfect specimen uniaxially by 0.1 mm before applying the prescribed experimental velocities. The value of 0.1 mm is chosen to make sure that the simulated initial peak is same as the one from experimental curve at uniaxial compression.

Quasi-static simulations are almost impossible to achieve with ABAQUS/Standard which uses Newton's method (or quasi Newton's method) as a numerical technique due to the complex nonlinear effects, e.g. the geometrical and material nonlinearity, the complex contact conditions as well as the local instability during crush. An alternative is to use also ABAQUS/Explicit for quasi-static problems. However, the explicit integration scheme of dynamic simulation codes usually leads to very small time step which in our simulation is around ten nanoseconds for the chosen element size. Thus, with the loading velocity of 0.1 mm/s, the computational duration for the quasi-static simulation (e.g. 180 s) will be too large. To overcome this difficulty, automatic mass scaling technique was employed to increase the time increment to 100 μs. The quasi-static loading conditions are guaranteed by ensuring the ratio of the kinetic energy to the strain energy as a small value (of the order of $10^{-4}$) with the chosen time increment.

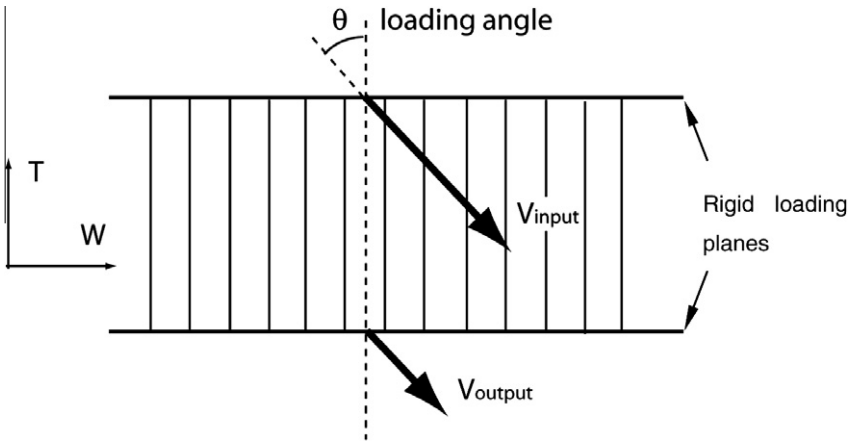


**Fig. 2.** Scheme of loading velocities.

**Table 1**
Bilinear material parameters.

| Material | Density $\rho$ (kg/m$^3$) | Young's modulus E (GPa) | Poission's ratio $v$ | Yield stress $\sigma_s$ (MPa) | Hardening modulus $E_t$ (MPa) |
|---|---|---|---|---|---|
| Aluminium | 2700 | 70 | 0.35 | 380 | 500 |

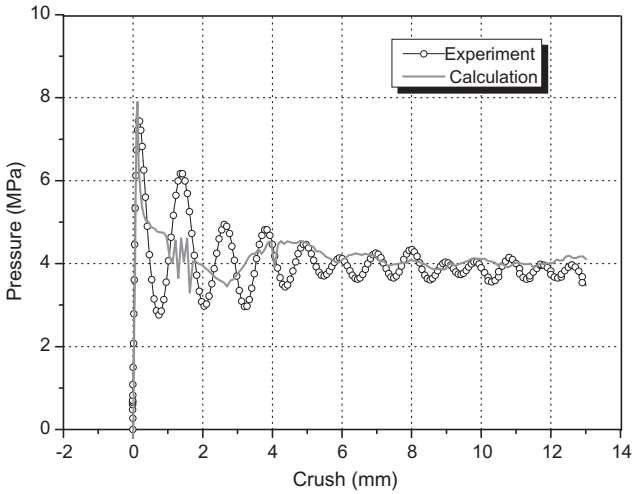


**Fig. 3.** Comparison between numerical and experimental results under uniaxial compression.

A bilinear elasto-plastic material model was employed to describe the cell wall material of this aluminum honeycomb. The model parameters of the base material such as yield stress and hardening modulus were determined by fitting the calculation result of uniaxial compression to the result from experiment (Table 1). Fig. 3 shows the comparison between experimental and simulated pressure/crush curves, which validates the parameters of this bilinear material model.

### 2.2. Simplified models

In order to reduce the calculation cost with this complete honeycomb model, numerical models with various simplifications can be also used. For example, some researchers (Papka and Kyriakides, 1999; Hönig and Stronge, 2002) used one-dimensional beam elements with different microsections for the simulation of the in-plane behavior, while some others employed one layer of shell element according to the repeated behavior in cell axis direction (Zou et al., 2009). As to the out-of-plane behavior, honeycomb specimen was usually simplified into a unit cell or a row of cells because of its periodicity (Mohr and Doyoyo, 2004b). However, these simplifications may introduce some imprecisions to the numerical model. In order to check the potential errors, two simplified models were also established. By comparing the results of these three models under uniaxial out-of-plane compression, the accuracy of the simplified numerical models will be evaluated.

The so called row-model is made up of a row of cells based on the periodicity of honeycomb specimen in *L*-direction (as shown in Fig. 4) and will be used to investigate the combined shear-compression behavior of honeycombs in *TW* plane. The most simplified model consists of three conjoint half walls in "*Y*" configuration (denoted as cell-model as in Fig. 4) and can be used only in uniaxial compression to make a comparison with the other two models. Both of the two simplified models have a length of 25 mm in *T*-direction, and the same element size of 0.25 mm as in the complete model. The numbers of elements for row-model and cell-model are 28,500 and 2100 respectively.

The simplified models work with symmetric boundary conditions. These displacement constraints are applied to the row-model on the two boundaries in *L*-direction (as shown in Fig. 4). For the cell-model, symmetric boundary conditions are performed on the three non-intersecting edges of each cell wall in local *y*-direction (as shown in Fig. 4). The same method is employed to introduce imperfections into these simplified models.

Fig. 5 shows a comparison of pressure/crush curves for the three models and the experiment. The row-model shows a good agreement with the complete-model while the cell-model exhibits significant fluctuations at the plateau stage which is probably due

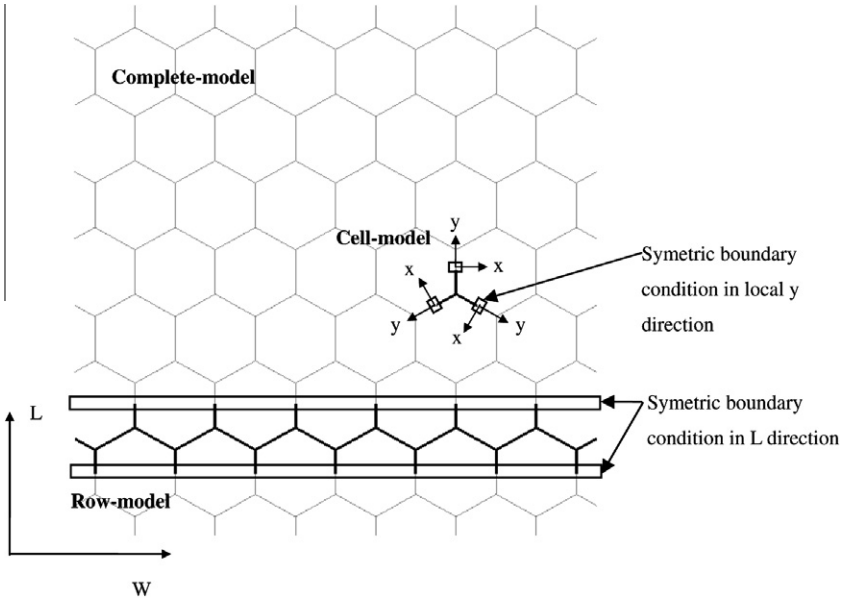


**Fig. 4.** Scheme of complete and simplified models.

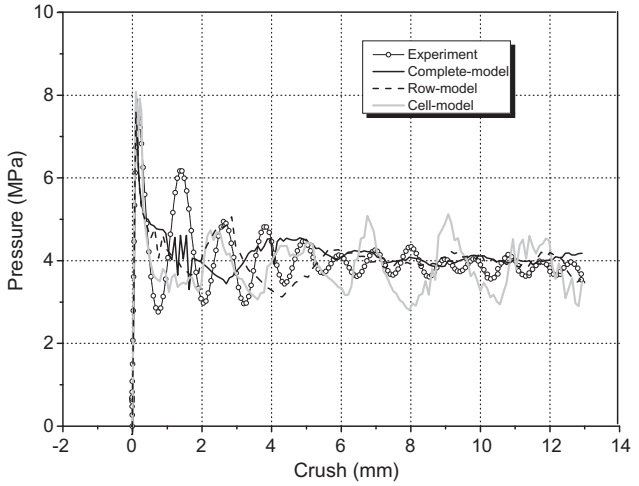


**Fig. 5.** Comparison between the calculating results from three models.

to the application of excessive symmetric boundary constraints. Actually, it is well known that the crushing behavior of honeycombs under out-of-plane compression is regulated by the successive folding procedure of honeycomb cell walls. With the symmetric boundary condition on three non-intersecting edges, the cell-model is actually equivalent to a honeycomb specimen consisting of repeated cells with identical deforming procedure, which results in strictly simultaneous collapse of all the honeycomb cells. Thus, in the pressure/crush curve, each fluctuation represents one fold formation of the cell wall in honeycomb microstructure. For the large size model, the neighboring cells interact with each other while forming the folds and reach their local peak value at different instants, which makes the macroscopic resulting curves smoother.

As a conclusion, the cell-model has some shortages in properly simulating the boundary conditions and fails to calculate the honeycomb multiaxial behavior. Although an ideal model should be of the same dimensions as the tested specimen, considering the contributions of simplified models in reducing the time-expense of calculation, we finally chose the row-model for the subsequent calculations on the biaxial behavior of honeycombs under combined shear-compression.

## 3. Biaxial behavior of honeycombs under combined shear-compression

In this section, the results of honeycomb under combined out-of-plane shear-compression (in *TW* plane) simulated with row-model are presented. It includes four loading angles of 30°, 40°, 50° and 60° and both dynamic and quasi-static loading cases. We first carefully examined the validity of our numerical specimen by comparing the overall pressure/crush curves and the deforming modes with experimental results at various loading angles. Finally, the normal and shear behaviors of numerical honeycombs under combined shear-compression can be separated.

### 3.1. Validation of numerical specimen

The overall pressure/crush curves are obtained from the calculated results in order to make a comparison between the experiments and the simulations. It is worth emphasizing that the variable "crush" is defined in Part I as the relative displacement component of the two moving bevels in $X_3$ direction and the "pressure" as the $X_3$ force component divided by specimen cross-sectional area $S_s$. As a consequence, in the case of numerical combined shear-compression test, the pressure $P(t)$ is calculated by dividing the contact force component in the rigid planes moving direction ($X_3$ direction in Fig. 6) with specimen area $S_s$. Its relationship with the directly obtained normal and shear contact forces is as follow:

$$P(t) = (F_n(t)\cos\theta + F_s(t)\sin\theta)/S_s, \tag{1}$$

where $\theta$ is the loading angle as defined in Part I. $F_n(t)$ and $F_s(t)$ are respectively the normal and shear contact forces at the interfaces of honeycomb specimen and rigid loading planes.

The overall crush $\Delta(t)$ is derived from the relative resultant displacement of the two reference points on rigid planes (Fig. 6). It has simple relationship with the normal and shear crushes (denoted as $d_n(t)$ and $d_s(t)$), which is:

$$\Delta(t) = d_n(t)/\cos\theta = d_s(t)/\sin\theta. \tag{2}$$

Fig. 7 presents the experimental and calculated pressure/crush curves under dynamic uniaxial compression and combined shear-compression for a loading angle $\theta = 50°$. Each curve has two distinct stages. During the stage I (from the beginning of zero crush to the position of the initial peak), the slopes of elastic segment are in good agreement for the calculations and the experiments. In addition, with the employed magnitude of imperfection, the initial peak of the calculated curve also agrees well with the experiment. During the stage II (defined as the following crush period after the stage I to 13 mm crush), the experimental curves have more fluctuations than the calculated ones, but the average strength is rather correct.

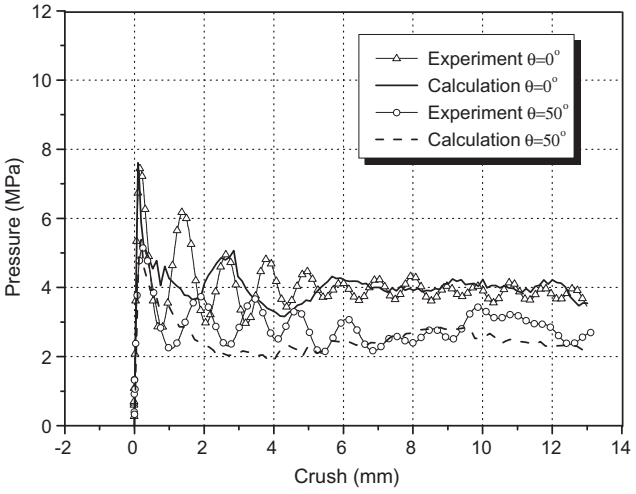


**Fig. 7.** Comparison of the dynamic pressure/crush curves from calculations and experiments.

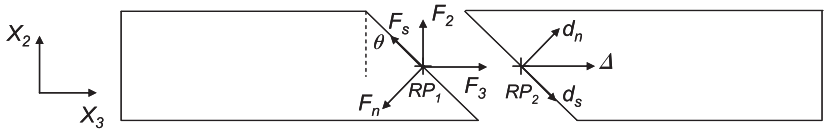


**Fig. 6.** Scheme of the decompositions of force and crush.

A comparison between the initial peak value as well as the average strength for every loading angle is described in Fig. 8. The average strength is defined as the curve area (absorbed energy) of this plateau stage divided by the corresponding crush length (the same formulas as used for experimental curves (Eq. (3) in Part I)):

$$\bar{p} = \frac{1}{\delta_{\max} - \delta^*} \int_{\delta^*}^{\delta_{\max}} p d\delta, \tag{3}$$

where $\delta^*$ denotes the crush value at the initial peak for each of the overall pressure/crush curve. $\delta_{\max}$ is the maximum crush.

A maximum difference of 4.9% between the simulation and the experiment is found for the initial peak at loading angle of 50°. For the average strength, the deviation from experiment is a little more significant at larger loading angles.

The quasi-static virtual testing results for uniaxial compression and combined shear-compression at loading angle $\theta = 50°$ are compared in Fig. 9 together with the experimental curves. The numerical results show a good correlation with the experimental ones at the crushing stage II. The average strengths are calculated for all the loading angles and listed in Fig. 10. The maximum difference of 13.2% is found at loading angle of 40°.

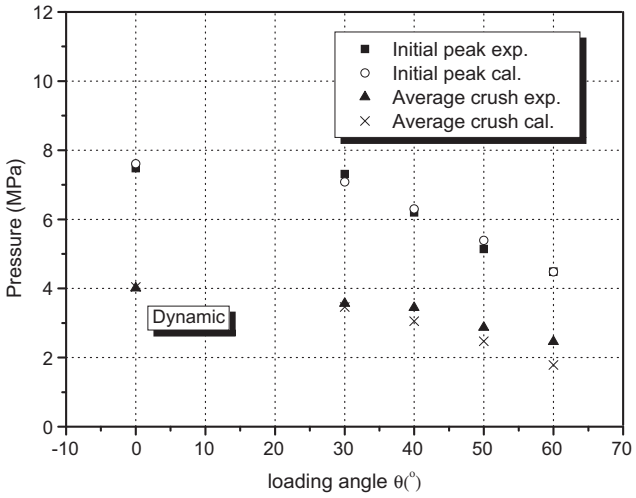


**Fig. 8.** Comparison of the initial peak and average strength between dynamic calculations and experiments at various loading angles.

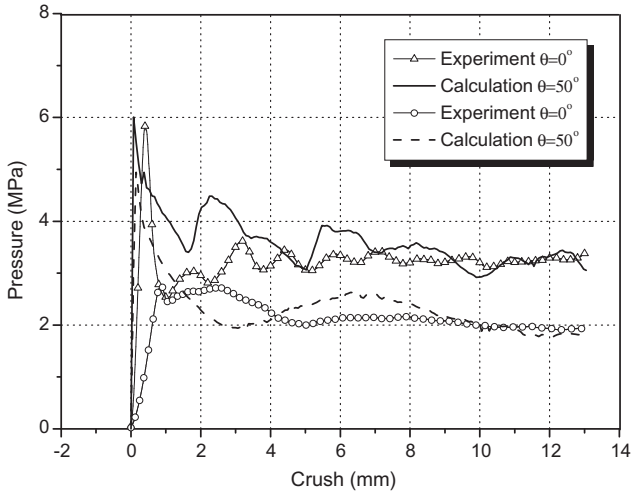


**Fig. 9.** Comparison of the quasi-static pressure/crush curves from calculation and experiments.

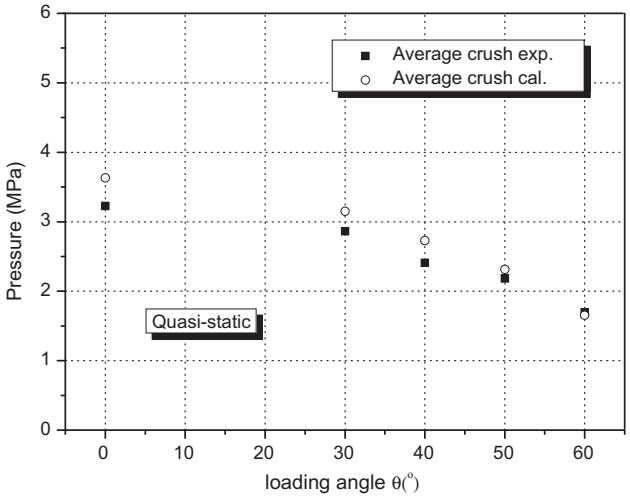


**Fig. 10.** Comparison of average strength between quasi-static calculations and experiments at various loading angles.

Nevertheless, during the stage I of the curves, a clear difference is found for both the ascending segment slope and the initial peak value that can be attributed to a slight slippage between specimen and bevels at the beginning of the experiment.

Furthermore, the simulated deforming pattern of honeycombs under combined shear-compression during the stage II is also compared with the experimental observations obtained with high speed camera. Fig. 11(a) and (b) show the specimens at dynamic loading of $\theta = 30°$ and at crush of 12 mm, and Fig. 11(c) and (d) for the quasi-static loading of $\theta = 50°$. It can be seen that the cell wall axis of all the displayed specimens incline during the crushing processes, and the inclined directions of the virtual and real specimens are in parallel to each other for the two different loading angles. Besides, the phenomenon of two-side folding system is also found in the numerical results as discovered for most of the experimental shear-compression specimens.

However, the numerical result can not cover at the same time the two deforming modes (rotation of cell axis or not) found during experiments (see Part I). Fig. 12 illustrates the rotation angle $\beta$ at 40% nominal compressive strain for every loading angle. It appears that our numerical specimen have a clear preference for the deforming mode with significant cell axis rotation.

### 3.2. Multiaxial behavior

The validation of the simulation work in Section 3.1 shows that the virtual testing results can represent well the experimental ones with the exception of quasi-static initial peak values. These virtual combined shear-compression tests provide more information than the real experiments and enable us to study separately the normal and shear behaviors of honeycombs.

The separated normal and shear pressure/crush curves under dynamic loading are shown in Fig. 13(a) and (b) respectively. It is noted that the normal and shear pressures are calculated from the normal and shear contact forces ($F_n(t)$ and $F_s(t)$) at the interfaces between rigid loading planes and honeycomb specimen. For the sake of clarity, only 0° (not included in shear behavior), 40° and 60° are displayed.

It is observed in Fig. 13(a) that the level of normal pressure/crush curves decreases when the loading angle increases. The shear behaviors are generally weaker than the normal ones (as shown in Fig. 13(b)) and their initial peak becomes inconspicuous with

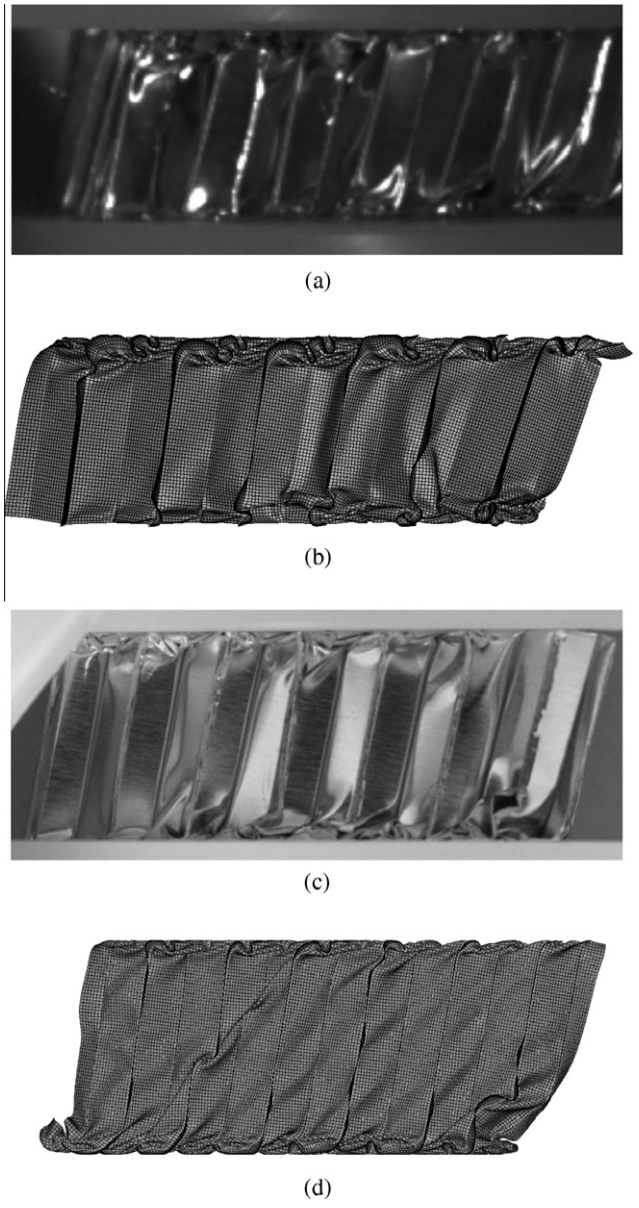


**Fig. 11.** Comparison of deformation configurations of experimental ((a) and (c)) and calculating ((b) and (d)) honeycomb specimens under dynamic ($\theta = 30°$ (a) and (b)) and quasi-static ($\theta = 50°$ (c) and (d)) combined shear-compression.

respect to the succeeding plateau. The level of the shear curves at the plateau stage increases with increasing loading angle, which shows an opposite trend to normal behavior.

It is worthwhile to recall that, the change of the loading angle in experiment modifies not only the ratio between normal and shear loadings but also the measured axis-force component. Here in this numerical test, such an ambiguity is eliminated because we measured directly the normal and shear strengths. The results shown in Fig. 13 do mean a lower resistance of honeycomb structure to compression under an increasing additional shear.

Under quasi-static loading, the normal and shear pressure/crush curves show a great similarity to the dynamic ones, i.e. the normal strength decreases with the loading angle whereas the shear strength increases. Moreover, a comparison between the quasi-static and the dynamic curves shows that the loading rate will also affect the normal and shear behaviors of honeycombs under combined shear-compression. Fig. 14 displays the dynamic and

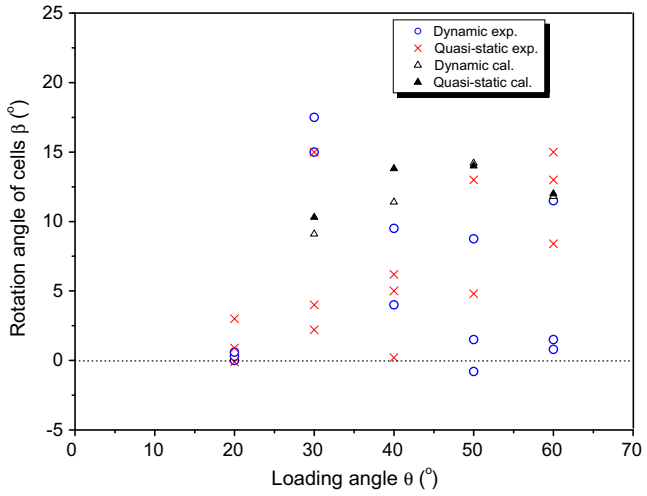


**Fig. 12.** Comparison of the cell axis rotation at every loading angle from both experiments and simulations.

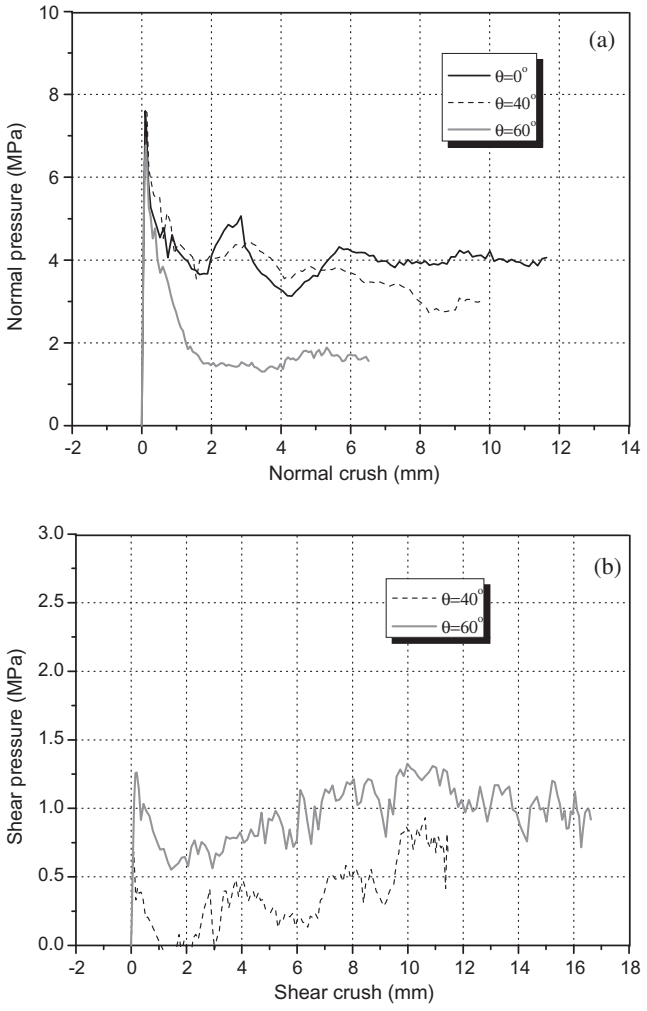


**Fig. 13.** Normal (a) and shear (b) behaviors of honeycomb under dynamic combined.

quasi-static normal and shear curves at $\theta = 40°$ and an enhancement is found for both of the two groups of curves.

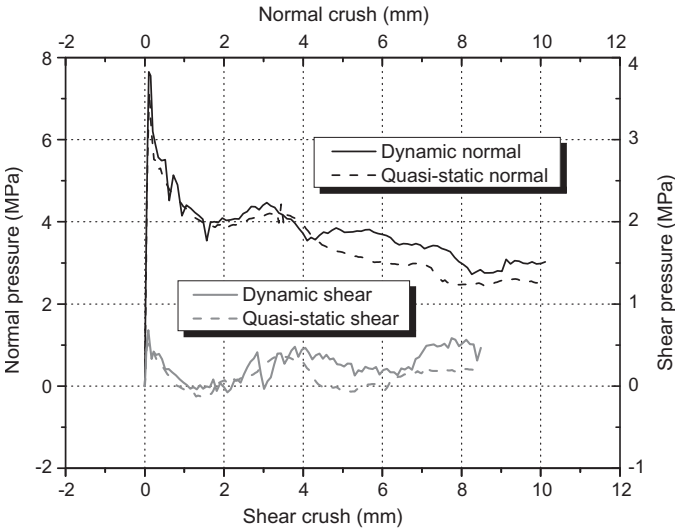


**Fig. 14.** Comparison between dynamic and quasi-static normal and shear pressure/crush curves at loading angle of 40°.

The average strengths of normal and shear behaviors were calculated for both dynamic and quasi-static loadings at every loading angle. All these average values are collected in Fig. 15, which shows clearly the change of the normal and shear strengths along with the loading angle as well as a strength enhancement under impact loading for every loading angle.

### 3.3. Macroscopic yield envelop estimation

Fig. 16 shows the distribution of calculated honeycomb biaxial behavior during the stage II on the normal average strength vs. shear average strength plane. An elliptical shape is found for both the quasi-static and dynamic loading cases (Eq. (4)).

$$\left(\frac{\sigma}{\sigma_0}\right)^2 + \left(\frac{\tau}{\tau_0}\right)^2 = 1, \tag{4}$$

where $\sigma_0$ and $\tau_0$ are respectively the normal strength under uniaxial compression and the shear strength under pure shear loading. By fitting the data with Levenberg–Marquardt algorithm (LMA), these two parameters are identified to be 3.98 MPa and 1.11 MPa under dynamic loading and 3.57 MPa and 1.02 MPa under quasi-static loading.

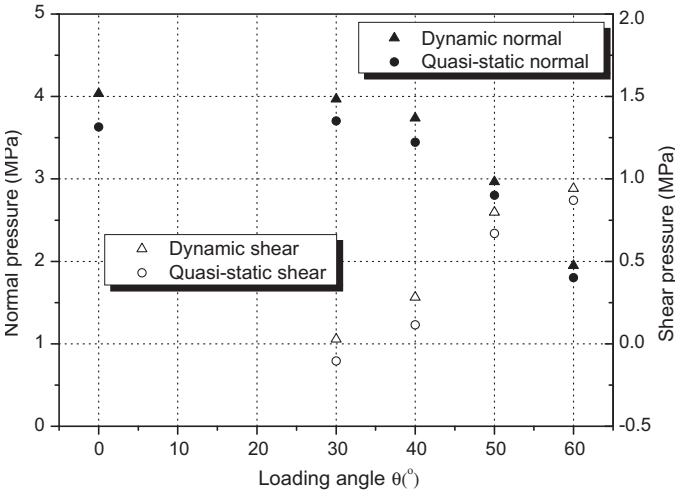


**Fig. 15.** Comparison between dynamic and quasi-static normal and shear pressure vs. loading angle.

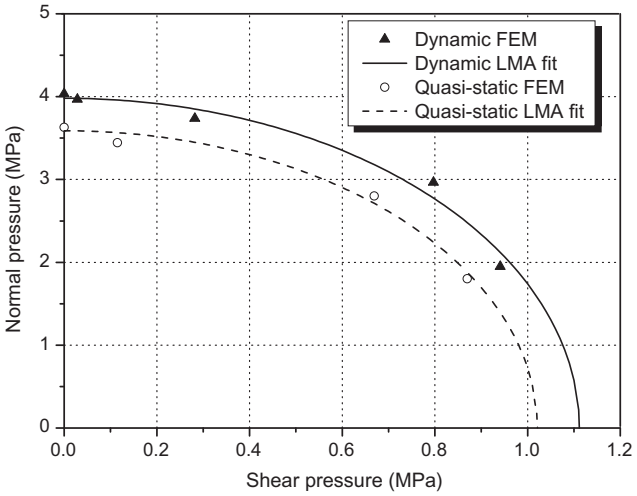


**Fig. 16.** Crushing envelopes of honeycomb in normal strength vs. shear strength plane.

It is found in Fig. 16 that the expansion of the crush envelope from the quasi-static loading to the dynamic loading is almost isotropic, even though the normal strength/shear strength ratio for a given loading angle is different under quasi-static and dynamic loading. It means that the dynamic biaxial strength for this honeycomb might be derived by using the enhancing ratio of uniaxial compression and the quasi-static crush envelope.

## 4. Conclusions

This study proposed a new method for investigating the dynamic biaxial behavior of honeycombs by combining the experiments based on SHPB technique and the FEM analyses.

A numerical specimen was built with a simplified row-model and identified material parameters. It provides simulated results in good agreement with the experiments in terms of deforming mode and the overall pressure/crush curves, which were the final information obtained from the new designed combined shear-compression experiments.

Such numerical virtual tests enabled to separate the normal and shear behaviors of honeycombs. It showed that the strength of honeycombs under compression is largely affected by the additional shear loading and exhibits a significant decrease while increasing shear loading. An obvious enhancement was also observed at dynamic loading for both normal and shear behaviors with respect to the quasi-static case at every loading angle.

In order to describe the dynamic and quasi-static biaxial behaviors of honeycombs at macroscopic level, an elliptical criterion in the plane of normal strength vs. shear strength can be derived with a set of parameters obtained by fitting the data with Levenberg–Marquardt algorithm. The expansion of the crush envelope with loading rate happened to be isotropic for this studied honeycomb in combined out-of-plane shear-compression.

## Acknowledgements

The authors thank 111 project of China (contract No.1307050) for funding the cooperation between NPU and LMT. B. Hou and Y. L. Li would also like to thank the supports of the National Science Foundation of China (contract No.10932008).

## References


Baker, W.E., Togami, T.C., Weydert, J.C., 1998. Static and dynamic properties of high-density metal honeycombs. Int. J. Impact Eng. 21, 149–163.

Chung, J., Waas, A.M., 2002. Compressive response of circular cell polycarbonate honeycombs under inplane biaxial static and dynamic loading. Part I: experiments. Int. J. Impact Eng. 27, 729–754.

Doyoyo, M., Mohr, D., 2003. Microstructural response of aluminum honeycomb to combined out-of-plane loading. Mech. Mater. 35, 865–876.

Elnasri, I., Pattofatto, S., Zhao, H., Tsitsiris, H., Hild, F., Girard, Y., 2007. Shock enhancement of cellular structures under impact loading: Part I experiments. J. Mech. Phys. Solids 55, 2652–2671.

Gibson, L.J., Ashby, M.F., 1997. Cellular Material: Structure and Properties, second ed. Cambridge University Press, Cambridge, UK.

Gibson, L.J., Ashby, M.F., Zhang, J., Triantafillou, T.C., 1989. Failure surfaces for cellular material under multiaxial loads-I. Modeling. Int. J. Mech. Sci. 31, 635–663.

Goldsmith, W., Louie, D.L., 1995. Axial perforation of aluminum honeycombs by projectiles. Int. J. Solids Struct. 32, 1017–1046.

Goldsmith, W., Sackman, J.L., 1992. An experimental study of energy absorption in impact on sandwich plates. Int. J. Impact Eng. 12, 241–262.

Harrigan, J.J., Reid, S.R., Peng, C., 1999. Inertia effects in impact energy absorbing materials and structures. Int. J. Impact Eng. 22, 955–979.

Hong, S.T., Pan, J., Tyan, T., Prasad, P., 2006. Quasi-static crush behavior of aluminum honeycomb specimens under compression dominant combined loads. Int. J. Plasticity 22, 73–109.

Hong, S.T., Pan, J., Tyan, T., Prasad, P., 2008. Dynamic crush behaviors of aluminum honeycomb specimens under compression dominant inclined loads. Int. J. Plasticity 24, 89–117.

Hönig, A., Stronge, W.J., 2002. In-plane dynamic crushing of honeycombs. Part I: crush band initiation and wave trapping. Int. J. Mech. Sci. 44, 1665–1696.

Klintworth, J.W., Stronge, W.J., 1988. Elasto-plastic yield limits and deformation laws for transversely crushed honeycombs. Int. J. Mech. Sci. 30, 273–292.

Mohr, D., Doyoyo, M., 2004a. Experimental investigation on the plasticity of hexagonal aluminium honeycomb under multiaxial loading. J. Appl. Mech. 71, 375–385.

Mohr, D., Doyoyo, M., 2004b. Deformation-induced folding systems in thin-walled monolithic hexagonal metallic honeycomb. Int. J. Solids Struct. 41, 3353–3377.

Mohr, D., Doyoyo, M., 2004c. Large plastic deformation of metallic honeycomb: orthotropic rate-independent constitutive model. Int. J. Solids Struct. 41, 4435–4456.

Papka, S.D., Kyriakides, S., 1999. In-plane biaxial crushing of honeycombs-Part II: analysis. Int. J. Solids Struct. 36, 4397–4423.

Wu, E., Jiang, W.S., 1997. Axial crush of metallic honeycombs. Int. J. Impact Eng. 19, 439–456.

Yang, M.Y., Huang, J.S., 2005. Elastic buckling of regular hexagonal honeycombs with plateau borders under biaxial compression. Compo. Struct. 71, 229–237.

Zhao, H., Gary, G., 1998. Crushing behaviour of aluminium honeycombs under impact loading. Int. J. Impact Eng. 21, 827–836.

Zhao, H., Elnasri, I., Abdennadher, S., 2005. An experimental study on the behavior under impact loading of metallic cellular materials. Int. J. Mech. Sci. 47, 757–774.

Zou, Z., Reid, S.R., Tan, P.J., Li, S., Harrigan, J.J., 2009. Dynamic crushing of honeycombs and features of shock fronts. Int. J. Impact Eng. 36, 165–176.